A strain gage method for determination of magnetic-moment intensity factors in through-cracked soft ferromagnetic plates

doi: 10.1063/1.1798400

A strain gage method for determination of magnetic-moment intensity factors in through-cracked soft ferromagnetic plates

Katsumi Horiguchi and Yasuhide Shindo[a)]
Department of Materials Processing, Graduate School of Engineering, Tohoku University, Aoba-yama 6–6–02, Sendai 980-8579, Japan

(Received 3 November 2003; accepted 3 August 2004)

This paper presents the results of a study on the effect of magnetic fields on the moment intensity factors in the through-cracked soft ferromagnetic plates with fixed ends. The experiments were conducted on a ferritic stainless steel with the through-cracked plate specimen geometries in a uniform, static transverse magnetic field. Strain gages were used to evaluate the magnetic-moment intensity factors. The experimental results were given for a single-internal crack, a single-edge crack, and two symmetric-edge cracks. The magnetic-moment intensity factor estimated from the measured strains was in good agreement with the theoretical calculations based on the authors' previous work. © *2004 American Institute of Physics*. [DOI: 10.1063/1.1798400]

I. INTRODUCTION

With the growing use of ferromagnetic steels in electromagnetic devices such as fusion reactors, the need for the fundamental understanding of the effect of magnetic fields on the fracture properties of the candidate structural materials becomes imperative. Incoloy (trademark of Inco Alloys International, Inc., Huntington, WV) alloy 908, a nickel-iron-based superalloy developed for the use in the Nb_3Sn superconducting magnets, is a candidate conduit material for the central solenoid and toroidal field coils of the International Thermonuclear Experimental Reactor.[1] Clatterbuck *et al.*[2] performed the compact tension fracture-toughness tests on the alloy 908, a ferromagnetic austenite, at a liquid-helium temperature in the magnetic fields of 0, 12, and 14 T (T:tesla). Using the notch tensile tests, Yamaguchi *et al.*[3] evaluated the fracture properties of the alloy 908 in cryogenic high magnetic-field environments. In these cases, the magnetic field was applied perpendicular to the plane of a crack or notch. They found that the fracture toughness was not significantly affected by the magnetic fields. To interpret the results, Yamaguchi *et al.*[3] reviewed the available theory of the influence of magnetic field on the stress intensity factor for a crack in the ferromagnetic materials.[4] The theoretical model predicted a negligible magnetic-field effect on the stress intensity factor for a crack in the low permeability materials.

Ferromagnetic ferritic/martensitic steels such as F82H(8Cr-2WVTa) and HT-9(12Cr-1MoVW) are being considered as the candidate first-wall materials for magnetic fusion reactors.[5] In many relatively thin-walled plate structures, the through cracks may develop as a result of cyclic loading. Following a classical plate-bending theory of magnetoelasticity, Shindo *et al.*[6] considered the crack problem of a soft ferromagnetic plate, which was permeated by a static uniform magnetic-field normal to the plate surface and was deformed by bending moments at the simply supported ends. They found that the magnetic-field effect can increase the values of the moment intensity factor. No experiments were reported in Ref. 6.

The primary objective of this study is to measure the magnetic-moment intensity factor in a ferritic stainless steel and verify the theoretical model presented in Ref. 6. The static experiments were conducted on the through-cracked plate specimens in the bore of a superconducting magnet at room temperature. A simple experimental technique employing strain gages was used to determine the magnetic-moment intensity factor.

II. REVIEW OF THE THEORY

We consider a soft ferromagnetic elastic plate of thickness $2h$, Poisson's ratio υ, Young's modulus E, flexural rigidity of the plate $D=2Eh^3/3(1-\upsilon^2)$, and magnetic susceptibility χ. The coordinate axes x and y are in the middle plane of the plate and the z axis is perpendicular to this plane. The plate is permeated by a static uniform magnetic field of a magnetic induction B_0 normal to the plate surface.

All the magnetic quantities are divided into two parts, those in the rigid body state and those in the perturbation state as follows:

$$B = B_0 + b, \quad H = H_0 + h, \quad M = M_0 + m, \tag{1}$$

where B, H, and M are the magnetic induction, magnetic intensity, and magnetization vectors, respectively. The first parts, which are indicated by the subscript 0, are the magnetic quantities in the undeformed body. The second parts, which are represented by the lower case letters, are the corrections to account for the additional changes in the magnetic quantities due to deformations. The solution to the problem of magnetostatics for the rigid body state is

$$B^e_{0_z} = B_0, \quad H^e_{0_z} = \frac{B_0}{\mu_0}, \quad M^e_{0_z} = 0 \quad (h < |z|), \tag{2}$$

[a)]Author to whom correspondence should be addressed; FAX: +81-22-217-7341; electronic mail: shindo@material.tohoku.ac.jp

$$B_{0_z} = B_0, \quad H_{0_z} = \frac{B_0}{\mu_0\mu_r}, \quad M_{0_z} = \frac{\chi B_0}{\mu_0\mu_r} \quad (|z| \leqslant h), \tag{3}$$

where B_{0_z}, H_{0_z}, and M_{0_z} are the z components of B_0, H_0, and M_0, respectively, the superscript e indicates the values outside the plate, $\mu_0 = 4\pi \times 10^{-7}$ N/A^2 (H/m; H: henry) is the magnetic permeability of the vacuum, and $\mu_\tau = 1 + \chi$ is the specific magnetic permeability. The magnetic equations for the perturbed state are satisfied by introducing a magnetic potential ϕ such that

$$h_x = \phi_{,x}, \quad h_y = \phi_{,y}, \quad h_z = \phi_{,z}, \tag{4}$$

$$\phi_{,xx} + \phi_{,yy} + \phi_{,zz} = 0, \tag{5}$$

where a comma denotes the partial differentiation with respect to the coordinate, h_x, h_y, and h_z are the x, y, and z components of h, respectively.

The classical plate-bending theory of magnetoelasticity is applied[6] and a dipole model for the magnetization is assumed.[7] The equations of equilibrium for a soft ferromagnetic plate under bending in a transverse uniform magnetic field can be written in the following form:

$$D(w_{,xxxx} + 2w_{,xxyy} + w_{,yyyy}) = m_{xx,x} + m_{yy,y} + q, \tag{6}$$

$$m_{xx} = [z\sigma_{zx}]_{-h}^{h} + \frac{2\chi B_0}{\mu_r}\int_{-h}^{h} z\phi_{,xz}\, dz,$$

$$m_{yy} = [z\sigma_{zy}]_{-h}^{h} + \frac{2\chi B_0}{\mu_r}\int_{-h}^{h} z\phi_{,yz}\, dz, \tag{7}$$

$$q = [\sigma_{zz}]_{-h}^{h} + \frac{2\chi B_0}{\mu_r}\int_{-h}^{h} \phi_{,zz}\, dz, \tag{8}$$

where $w(x,y)$ represents the deflection of the middle plane of the plate, m_{xx} and m_{yy} are the resultant external moments, q is the external load, and σ_{zz}, $\sigma_{yz} = \sigma_{zy}$, and $\sigma_{zx} = \sigma_{xz}$ are the elastic stress components. The boundary conditions are given by

$$\sigma_{zx} = -\frac{\chi B_0}{\mu_r}\phi_{,x} \quad (|z| = h),$$

$$\sigma_{zy} = -\frac{\chi B_0}{\mu_r}\phi_{,y} \quad (|z| = h),$$

$$\sigma_{zz} = \frac{\chi(\chi - 2)}{\mu_r}\left\{\frac{B_0^2}{2\mu_0\mu_r} + B_0\phi_{,z}\right\} \quad (|z| = h), \tag{9}$$

$$\phi_{,z}^e - \mu_r\phi_{,z} = 0 \quad (|z| = h), \tag{10}$$

$$\phi_{,x}^e - \phi_{,x} = -\frac{\chi B_0}{\mu_0\mu_r}w_{,x} \quad (|z| = h),$$

$$\phi_{,y}^e - \phi_{,y} = -\frac{\chi B_0}{\mu_0\mu_r}w_{,y} \quad (|z| = h). \tag{11}$$

Consider a fixed-end soft ferromagnetic elastic plate of length l containing a through crack of length $2a$. The crack is located on the line $y = 0$, $|x| < a$. The cracked plate is bent by a normal line load P applied at the middle of the span. By the use of the Fourier transforms, we reduce the problem by solving a pair of dual-integral equations. The solution of the dual-integral equations is then expressed in terms of a Fredholm integral equation of the second kind. The moment intensity factor is obtained as

$$K_1 = \lim_{x \to a+}\{2(x - a)\}^{1/2} M_{yy}(x,0) = M_{0y}a^{1/2}\Phi(1), \tag{12}$$

where M_{yy} is the bending moment per unit length and

$$M_{0y} = M_{yy}(x,0) = 2Pl\sum_{n=1,3,5,\cdots}^{\infty} \frac{(2n\pi)\cos(n\pi)^2}{(2n\pi)^3 + B_n\left(\frac{l}{h}\right)^3\left\{(\chi + 2)\sinh\left(\frac{2n\pi}{l}h\right) - (2n\pi)\frac{h}{l}\cosh\left(\frac{2n\pi}{l}h\right)\right\}}, \tag{13}$$

$$B_n = -\frac{3(1 - \upsilon)\chi^2}{2\mu_r^2\{\mu_r \sinh(\alpha_n h) + \cosh(\alpha_n h)\}}b_c^2, \tag{14}$$

$$b_c^2 = \frac{2(1 + \upsilon)B_0^2}{\mu_0 E}, \tag{15}$$

$$\alpha_n = \frac{2n\pi}{l}. \tag{16}$$

The function Φ in Eq. (12) is the solution to the following Fredholm integral equation of the second kind:

$$\Phi(\xi) + \int_0^1 L(\xi,\eta)\Phi(\eta)d\eta = \xi^{1/2}. \tag{17}$$

The kernel $L(\xi,\eta)$ is given by

$$L(\xi,\eta) = \int_0^\infty (\eta\xi)^{1/2}\left\{\frac{f_1\left(\frac{\rho}{a}\right)}{f_0} - 1\right\}\rho J_0(\rho\eta)J_0(\rho\xi)d\rho, \tag{18}$$

where $J_0()$ is the zero-order Bessel function of the first kind and

$$f_1(\alpha) = \frac{1}{\alpha G(\alpha)}\left[\frac{(\gamma_1^2 - \upsilon\alpha^2)}{\gamma_1\{(\upsilon-2)\alpha^2 + \gamma_1^2\}} + \frac{(\gamma_2^2 - \upsilon\alpha^2)}{\gamma_2\{(\upsilon-2)\alpha^2 + \gamma_2^2\}}\right], \tag{19}$$

$$G(\alpha) = -\frac{1}{(\upsilon-2)\alpha^2 + \gamma_1^2} + \frac{1}{(\upsilon-2)\alpha^2 + \gamma_2^2}, \tag{20}$$

$$f_0 = \lim_{\alpha\to\infty} f_1(\alpha). \tag{21}$$

γ_j $(j=1,2)$ in Eqs. (19) and (20) are the roots of the following characteristic equation:

$$\left(\alpha^2 - \gamma_j^2\right)\left\{\mu_r\left(\alpha^2 - \gamma_j^2\right)^{1/2}h + 1\right\} - \frac{2\chi^2 B_0^2}{\mu_0\mu_r D}h = 0 \quad (j=1,2). \tag{22}$$

III. EXPERIMENTAL PROCEDURE

A. Material and specimens

Ferritic stainless-steel SUS430 was used as a specimen material. The Young's modulus, Poisson's ratio, and specific magnetic permeability were taken to be $E=162.3$ GPa, $\upsilon=0.294$,[8] and $\mu_\tau=122.9$. The Young's modulus was determined from the data on deflection for the cantilever specimen (100-mm-long by 40-mm-wide by 1-mm-thick) bent by a concentrated load applied at the end. The specific magnetic permeability was also measured with a vibrating sample magnetometer. The specimen geometries used were the single-internal crack, single-edge crack, and two symmetric-edge cracks. The specimen dimensions and the strain gage location are shown in Fig. 1. The length, width, thickness, and crack length of the specimen are l, W, $2h$, and $2a$, respectively. A five-element strip gage was installed along the 90°-line, and the center point of the element closest to the crack tip was 2 mm. The gages used in this work were KFG-1-120-D19-16 from the Kyowa Electronic Instruments Co., Ltd., Japan. The sensors on this type of strip gage have an active length of 1 mm and are on the 2-mm centers.

B. Testing method

The values of K_1 may be evaluated conveniently by measuring the local strain at selected positions.[9] A schematic diagram of the experimental setup used in this investigation is shown in Fig. 2. A superconducting magnet SM-3 with a 220-mm diameter bore at the High Field Laboratory for Superconducting Materials, Institute for Materials Research, Tohoku University was used to create a magnetic field of magnetic induction B_0 normal to the wide face of the specimen. The fixed-end through-cracked specimen was bent by a normal line load P, which consisted of weights. This line load was applied at the center of the plate. The experiments were conducted by sweeping the magnetic field at room temperature and measuring the strain. The strain gage response in the presence of the magnetic field was measured by loading a dummy aluminum specimen. The effect of the magnetic field on the strain gage response was negligible.

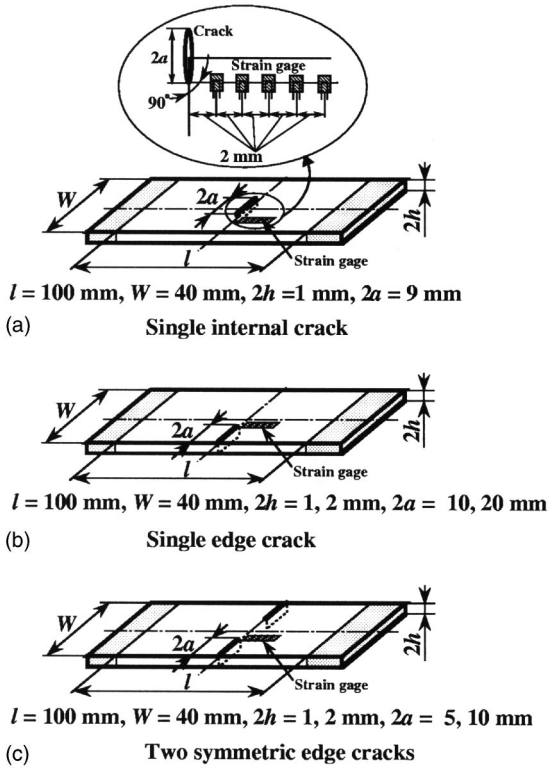

FIG. 1. Geometry and dimensions for the (a) single-internal crack, (b) single-edge crack, and (c) two symmetric-edge crack specimen.

C. Determination of moment intensity factor

We consider an elastic plate containing a through crack. The crack length $2a$ is assumed to be large in comparison with the plate thickness $2h$. The middle plane bisecting the plate thickness, as shown in Fig. 3, is usually taken as a reference. The coordinate axes x and y are in the middle plane of the plate, the z axis is perpendicular to this plane, and the polar coordinates r, θ are used to define the position of an element. In the standard theory of the thin plates under bending, the stresses near the crack tip are given by[10,11]

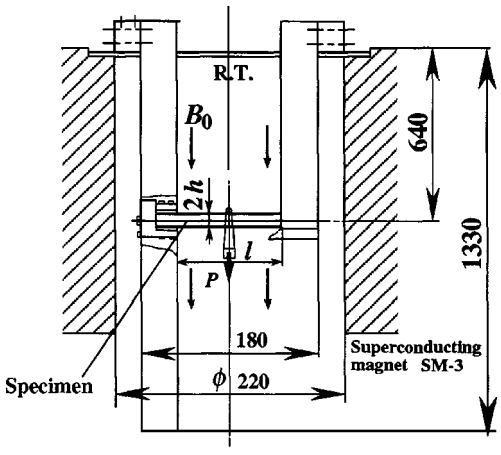

FIG. 2. Schematic of the experimental setup.

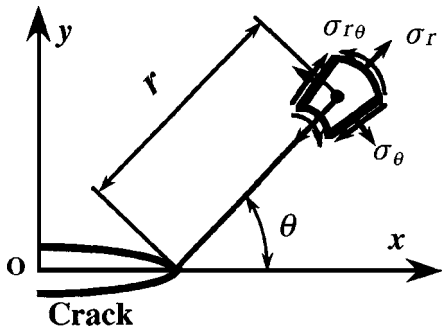

FIG. 3. Notation for the polar stress components near the crack tip.

$$\sigma_r = -\frac{k_1}{(2r)^{1/2}}\left\{\cos\left(\frac{3\theta}{2}\right) - \frac{3+5\nu}{7+\nu}\cos\left(\frac{\theta}{2}\right)\right\}\frac{(7+\nu)z}{4(3+\nu)h} - 4zA\{1+\cos(2\theta)\} + O(r^{1/2}),$$

$$\sigma_\theta = \frac{k_1}{(2r)^{1/2}}\left\{\cos\left(\frac{3\theta}{2}\right) + \frac{5+3\nu}{7+\nu}\cos\left(\frac{\theta}{2}\right)\right\}\frac{(7+\nu)z}{4(3+\nu)h} - 4zA\{1-\cos(2\theta)\} + O(r^{1/2}),$$

$$\sigma_{r\theta} = \frac{k_1}{(2r)^{1/2}}\left\{\sin\left(\frac{3\theta}{2}\right) + \frac{1-\nu}{7+\nu}\sin\left(\frac{\theta}{2}\right)\right\}\frac{(7+\nu)z}{4(3+\nu)h} + 4zA\sin(2\theta) + O(r^{1/2}), \quad (23)$$

where σ_r, σ_θ, and $\sigma_{r\theta}$ are the bending stresses and A is the constant. The bending stress intensity factor k_1 is defined by

$$k_1 = \lim_{r\to 0+}(2r)^{1/2}\sigma_\theta(r,0,h). \quad (24)$$

Substituting Eq. (23) into the stress σ, the strain ε relations gives

$$E\varepsilon_r = \sigma_r - \nu\sigma_\theta = -\frac{k_1(1+\nu)z}{4(3+\nu)h}\left\{(7+\nu)\cos\left(\frac{3\theta}{2}\right) + 3(\nu-1)\cos\left(\frac{\theta}{2}\right)\right\}(2r)^{-1/2} - 4z\{(1-\nu)+(1+\nu)\cos(2\theta)\}A + \cdots, \quad (25)$$

where ε_r is the radial strain. Setting $\theta=\pi/2$ and $z=h$ gives

$$a_0 E\varepsilon_r r^{1/2} = k_1 + 8h\nu a_0 A r^{1/2} + \cdots, \quad (26)$$

where

$$a_0 = \frac{4(3+\nu)}{(5-\nu)(1+\nu)}. \quad (27)$$

From Eq. (26), a plot of $a_0 E\varepsilon_r r^{1/2}$ versus $r^{1/2}$ is linear for the small values of r, and the intercept at $r=0$, at the crack front, gives the bending stress the intensity factor k_1. Since the stresses σ_r, σ_θ, and $\sigma_{r\theta}$ are related to the moments per unit length M_r, M_θ, and $M_{r\theta}$ by the relations

$$\sigma_r = \frac{3z}{2h^3}M_r, \quad \sigma_\theta = \frac{3z}{2h^3}M_\theta, \quad \sigma_{r\theta} = \frac{3z}{2h^3}M_{r\theta}, \quad (28)$$

the moment intensity factor K_1 may be obtained by multiplying k_1 by the factor $2h^2/3$.

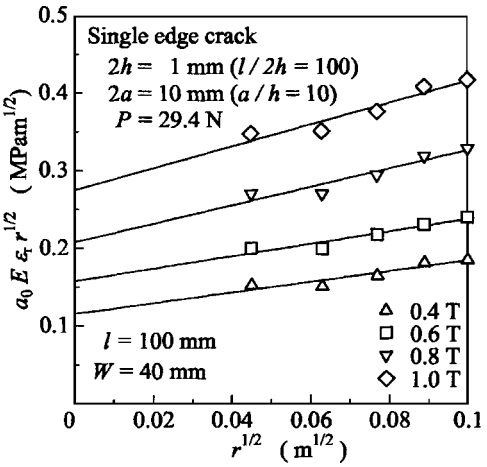

FIG. 4. Strain data for K_1 as a function of the position $r^{1/2}$.

IV. RESULT AND DISCUSSION

From the measured strain readings, a plot of $a_0 E\varepsilon_r r^{1/2}$ versus $r^{1/2}$ is constructed, as shown in Fig. 4. The moment intensity factor K_1 is obtained from the intercept of the $a_0 E\varepsilon_r r^{1/2}$ versus $\tau^{1/2}$ at $\tau=0$. A plot of the moment intensity factor with the magnetic field showing both the theoretical solution (solid line) and the experimental data (open symbols) is given in Fig. 5 for the single-internal crack specimen ($l/2h=100$, $a/h=9$, $P=29.4$, and 49.0 N). In this figure, the moment intensity factor is normalized with respect to K_{10}, which is the corresponding value for $B_0=0$. The experiments show the predicted increase in the moment intensity factor with an increasing magnetic field. No dependence of the moment intensity factor with the magnetic field on the load P is observed. The theoretical results agree very well with the experimental data. It may be observed that the result obtained from the theoretical model based on a classical plate-bending theory of magnetoelasticity in a soft ferromagnetic material is quite acceptable. Figure 6 shows the effect of the crack length $2a$ and the magnetic field B_0 on the moment intensity factor for the single-edge crack specimen ($l/2h=50$, $a/h=5,10$, and $P=29.4$ N). The magnetic-field effect can increase the values of the moment intensity factor and

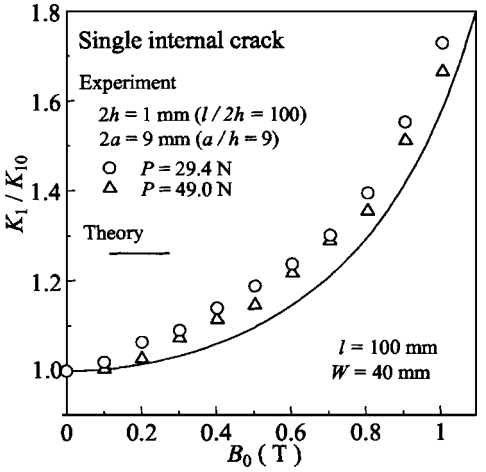

FIG. 5. Comparison of the measured magnetic-moment intensity factor with the theoretical result (single-internal crack).

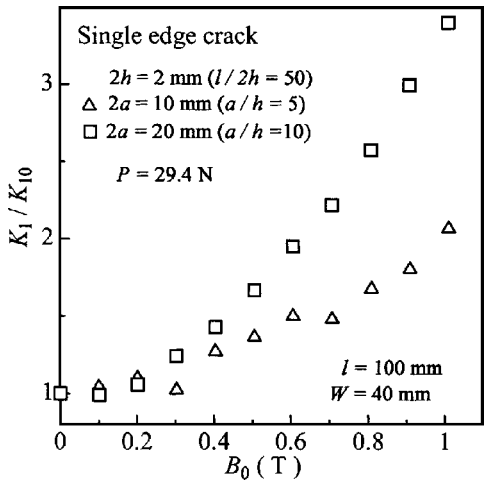

FIG. 6. Moment intensity factor vs magnetic field (single-edge crack).

depends on a/h. The moment intensity factors obtained for the two symmetric-edge cracks ($l/2h=50$, $a/h=2.5,5$; $l/2h=100$, $a/h=10$; $P=19.6$ N) are plotted as a function of the magnetic field in Fig. 7. An increasing trend in the moment intensity factor is observed. The effect of the magnetic field on the moment intensity factor is more pronounced with an increasing $l/2h$.

In the usual experimental case, the tensile load and magnetic field are perpendicular to the crack surface and parallel to the wide face of the CT (compact tension) specimen. The fracture toughness of the alloy 908 was not affected by even very high fields (14 T).[2] Shindo[4] investigated the two-dimensional crack problem for the soft ferromagnetic elastic solid subjected to a uniform magnetic field of the magnetic induction B_0, normal to the crack surface under the assumption of a plane strain. In this study, the solution to the problem was obtained for the uniform pressure σ_0 applied to the crack surface, which corresponds to the uniform far-field tension applied to the solid. The stress intensity factor k_{h1}, in this case, is determined as

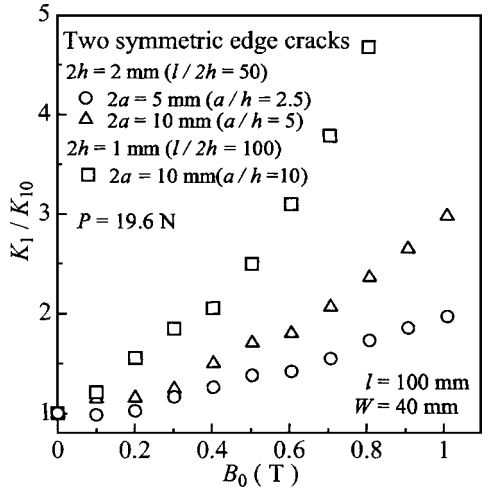

FIG. 7. Moment intensity factor vs magnetic field (two symmetric-edge cracks).

$$\frac{k_{h1}}{\sigma_0 c^{1/2}} = \frac{2\mu_r^2 + \{2(1-\nu) + (5-6\nu)\chi\}\chi b_c^2}{2\mu_r^2 - \{2(1-\nu)\chi - 1 + 2\nu\}(\chi b_c)^2}, \tag{29}$$

where c is the half-length crack. The mechanical and magnetic properties of SUS430 are $E=162.3$ GPa, $\nu=0.294$, and $\mu_r=122.9$ and the saturation magnetic field $B_S=1.5$ T. Using these values, Eq. (29) predicts a normalized stress intensity factor, $k_{h1}/\sigma_0 c^{1/2}=1.0025$. Let the specific magnetic permeability μ_r be changed, keeping all the other factors the same. To achieve a normalized stress intensity factor of 1.1, we must increase the specific magnetic permeability to 4600. We assume that the mechanical and magnetic properties of $E=175$ GPa, $\nu=0.28$, $\mu_r=10$, and $B_S=2$ T are typical for the alloy 908. If B_0 is increased to the saturation magnetic field of $B_S=2$ T, the value of $k_{h1}/\sigma_0 c^{1/2}$ becomes 1.0003. Since iron-based alloys will saturate if the magnetic induction is much over 2 T, lowering the permeability, we would not expect a magnetic field to have a significant effect on the stress intensity factor.

We again consider the single-internal crack problem of a fixed-end soft ferromagnetic plate ($l/2h=100$, $a/h=9$), which is permeated by a static uniform magnetic field normal to the plate surface and parallel to the crack surface and is bent by a normal line load applied at the middle of the span. Because drastic changes of the magnetic field can occur at a boundary, deformation or movement of a surface provides a primary coupling between the magnetic field and the deformation of the structure. The existence of a transverse magnetic field produces larger values of the deflection. The values of K_1/K_{10} for the saturation magnetic field are 4.1622 ($B_S=1.5$ T) and 1.1731 ($B_S=2$ T) for the SUS430 and Incoloy 908, respectively. The bending tests performed in this study used cracked thin plates in a transverse magnetic field, whereas the fracture-toughness tests conducted by Clatterbuck *et al.*[2] employed the CT specimens, which are loaded under tension in a magnetic field normal to the crack surface and parallel to the specimen wide surface. The magnetic-field effect on the fracture mechanics parameters depends on the direction of the magnetic field and the loading condition.

V. CONCLUSIONS

An experimental study has been conducted in which the strain fields were used to characterize the moment intensity factor under a magnetic field. The effect of the magnetic fields on the moment intensity factors has been summarized in a drawing. The existence of the magnetic field produces larger values of the moment intensity factor. This effect becomes more pronounced as the specimen length to a thickness ratio of $l/2h$ and the crack length to a thickness ratio of a/h increase. A close agreement between the theoretical prediction and the experimental data verifies the validity of the theory.

[1]M. M. Morra, R. G. Ballinger, and I. S. Hwang, Metall. Trans. A **23**, 3177 (1992).
[2]D. M. Clatterbuck, J. W. Chan, and J. W. Morris, Jr., Mater. Trans., JIM **41**, 888 (2000).
[3]Y. Yamaguchi, K. Horiguchi, Y. Shindo, D. Sekiya, and S. Kumagai, Cryogenics **43**, 469 (2003).

[4]Y. Shindo, ASME J. Appl. Mech. **44**, 47 (1977).
[5]R. L. Klueh, E. T. Cheng, M. L. Grossbech, and E. E. Bloom, J. Nucl. Mater. **280**, 353 (2000).
[6]Y. Shindo, K. Horiguchi, and T. Shindo, Int. J. Eng. Sci. **37**, 687 (1999).
[7]Y.-H. Pao and C.-S. Yeh, Int. J. Eng. Sci. **11**, 415 (1973).
[8]R. P. Reed and A. F. Clark, *Materials at low temperatures* (American Society for Metals, Metals Park, Ohio, 1983).
[9]J. W. Dally and R. J. Sanford, Exp. Mech. **27**, 381 (1987).
[10]W. J. Williams, ASME J. Appl. Mech. **28**, 78 (1961).
[11]G. C. Sih, ASME J. Eng. Ind. **92**, 350 (1970).